Materials Chemistry and Physics 234 (2019) 67–74

Contents lists available at ScienceDirect

Materials Chemistry and Physics

journal homepage: www.elsevier.com/locate/matchemphys

Surface-covalent functionalized graphene oxide sheets with hyperbranched polysiloxane and Mn ion for cyanate ester resin: Towards lower curing temperature and higher performance

Tianyu Cai, Li Yuan, Guozheng Liang *, Hong Wang, Aijuan Gu **

State and Local Joint Engineering Laboratory for Novel Functional Polymeric Materials, Jiangsu Key Laboratory of Advanced Functional Polymer Design and Application, Department of Materials Science and Engineering, College of Chemistry, Chemical Engineering and Materials Science, Soochow University, Suzhou, 215123, PR China

HIGHLIGHTS

- Surface-functionalized graphene oxide (HBP@GO/MnF) was fabricated.
- HBP@GO/MnF has good dispersion and interfacial interaction with bisphenol A dicyanate (BCy).
- HBP@GO/MnF makes BCy cured at lower curing temperature.
- HBP@GO/MnF/BCy resins have higher performances than BCy resin.
- The mechanisms behind these outstanding performances were systematically studied.

GRAPHICAL ABSTRACT

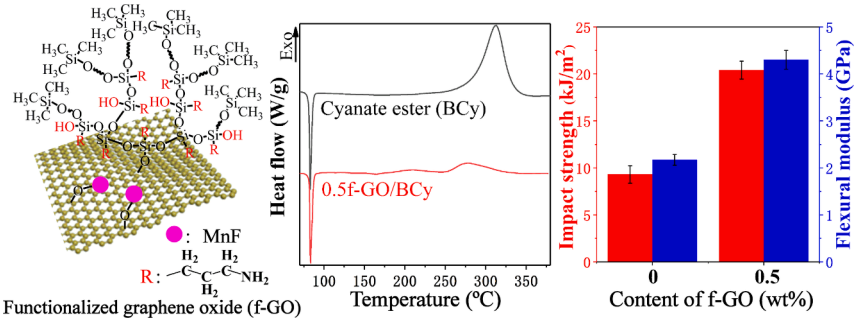

ARTICLE INFO

Keywords:
Hyperbranched polysiloxane
Surface
Cyanate ester
Nanocomposites
Interface

ABSTRACT

Achieving lower curing temperature and higher properties has been the significant target for developing heat-resistant thermosetting resins. Herein, a facile covalent approach has been built to fabricate functionalized graphene oxide (HBP@GO/MnF) through grafting hyperbranched polysiloxane (HBP) and hybridizing metal–organic framework with Mn^{2+} (MnF), which has been proved to have desirable abilities of simultaneously decreasing curing temperature as well as improving toughness and stiffness while maintaining the biggest advantage (low dielectric loss) and high thermal resistance of cyanate ester (BCy) resin. A comparative study demonstrates that the activation from HBP endows HBP@GO/MnF with good dispersion in BCy resin and provides strong interfacial action between HBP@GO/MnF and BCy resin. When the loading of HBP@GO/MnF is as small as 0.5 wt%, the peak temperature of curing reduces to 278 °C from 313 °C of BCy, meanwhile severally about 60%, 98%, 120% and 93% increased flexural strength, flexural modulus, impact strength and fracture toughness are achieved. In addition, all modified BCy resins post-cured at 220 °C/4 h have better mechanical properties and higher heat resistance than pure BCy resin post-cured at 240 °C for 4 h. These outstanding performances prove that HBP@GO/MnF is promising filler for fabricating new resins with higher performances and better curing feature.

* Corresponding author.
** Corresponding author.
E-mail addresses: lgzheng@suda.edu.cn (G. Liang), ajgu@suda.edu.cn (A. Gu).

https://doi.org/10.1016/j.matchemphys.2019.05.090
Received 26 February 2019; Received in revised form 20 May 2019; Accepted 27 May 2019
Available online 28 May 2019

1. Introduction

Thermally resistant resins (TRRs) have been increasingly required to fabricate high-level products in many cutting-edge fields such as aircrafts with higher Mach number, engines with higher power generation, electric products with faster transmission rates of signals and smaller dimensions, *etc.* [1–5]. However, TRRs are usually cured at high temperature to get outstanding integrated performances except for big brittleness [6–8], resulting in poor processing feature, high energy consumption and poor service reliability of related products. Therefore, simultaneously reducing curing temperature and improving toughness have always been an important topic in developing heat-resistant thermosetting resins.

Cyanate ester resin is representative of TRRs [9,10], which also has the common shortcomings of TRRs, namely high curing temperature and great brittleness. Different from other TRRs, cyanate ester resin has two unique natures. Very low dielectric loss at different frequencies is the first virtue [11]; however, note that dielectric property is sensitive to the composition of resins, so the chemical structure of modified resin should be carefully designed to maintain this advantage. The other is that –OCN group is very active, and will react with many groups [12–15]; however, the resulting co-polymers tend to have poorer performance than homopolymer of cyanate ester [16]. Therefore, it is more difficult to simultaneously solve two bottlenecks of reducing curing temperature and improving toughness for cyanate ester resin than other thermosetting resins.

Adding a curing catalyst is a common method to reduce curing temperature of TRRs. There are three kinds of curing catalysts of cyanate ester resin; they are active hydrogen compounds (phenol, amine, *etc.*) [17,18], organotin (dibutyltin dilaurate) [19,20], catalytic system consisting of transition metal salts (cobalt acetylacetonate, zinc octoate, *etc.*) and nonylphenol [21,22]. Among these catalysts, transition metal salt/nonylphenol mixed catalytic system has the highest catalytic efficiency [23], however, nonylphenol is a permanent poison listed by the United Nations Environmental Program in 1999 [24]. Therefore, it is necessary and valuable to design and synthesize new curing catalysts based on transition metal salt without using nonylphenol for cyanate ester resin.

In recent years, rigid inorganic nano-fillers have been widely used to toughen thermosetting resins. With this method, toughening is usually achieved at a low filler content (<5 wt%) while maintaining the stiffness and heat resistance of resins [25–27]. However, generally, rigid inorganic nano-fillers almost have no reactive groups and tend to form agglomeration due to large specific surface and high surface energy [28]. These shortcomings prevent inorganic nano-fillers from effectively exerting their toughening effect.

Graphene oxide (GO) is a distinctive rigid inorganic nano-filler, which has reactive groups including hydroxyl, carboxyl and epoxy groups on its surface, these groups are very beneficial for catalyzing self-polymerization of –OCN [15,29]. However, the amount of these reactive groups on the surface of GO is not enough to simultaneously produce an effective catalytic intermediate with transition metal salt, and also cannot ensure good dispersion of GO in resin.

We aim at designing and preparing a novel kind of functional filler, which not only acts as an intrinsic transition metal salt catalyst, but also an effective toughening modifier for cyanate ester resin, and consequently, overcoming two bottlenecks (high curing temperature and brittleness) while maintaining outstanding dielectric and thermal advantages of cyanate ester resin. Specifically, utilizing the advantages of hyperbranched polysiloxane (HBP) including enlarging the amount of reactive groups (amino and hydroxyl), high thermal stability and toughening ability, HBP grafted GO was synthesized to simultaneously satisfying requirements of improving interfacial interactions between GO and cyanate ester resin as well as acting as a co-catalyst of transition metal salt. Modified GO (HBP@GO) was then bonded with Mn^{2+} in metal–organic framework (MnF) to synthesize a novel hybrid (HBP@GO/MnF) with catalytic effect. The effect and mechanism of HBP@GO/MnF on integrated performances of cyanate ester resin were intensively studied.

Table 1
Compositions of HBP@GO/MnF/BCy resins.

Resin	Weight ratio	
	BCy	HBP@GO/MnF
BCy	100	0
f-BCy	100	0
0.5HBP@GO/MnF/BCy	100	0.5
1HBP@GO/MnF/BCy	100	1
2HBP@GO/MnF/BCy	100	2
4HBP@GO/MnF/BCy	100	4

2. Experimental

2.1. Chemical agents

Cyanate ester used was bisphenol A dicyanate (BCy) with industrial grade, which was made in Yangzhou Techia Material Co., Ltd., China. (3-Aminopropyl)triethoxysilane (APTES) was bought from Shanghai Aladdin Bio-Chem Technology Co., Ltd., China. Hexamethyldisiloxane was provided by Iota Silicone Oil Co., Ltd., China. Concentrated sulfuric acid (H_2SO_4, 98%), $NaNO_3$, $KMnO_4$, KOH, imidazole ($C_3N_2H_5$) and Mn $(OAc)_2{\cdot}4H_2O$ with analysis grades were commercial products. 4,4′-Dicarboxydiphenyl ether (98%) was purchased from Shanghai Chemical Reagent Co., Ltd., China. Graphene oxide (GO) was prepared from natural graphite powders according to the method of Hummers and Offeman [30].

2.2. Synthesis of hyperbranched polysiloxane grafted GO (HBP@GO)

APTES (10 mL), ethanol (100 mL) and deionized water (10 mL) were thoroughly blended and kept at 50 °C for 7 h to form a solution, into which hexamethyldisiloxane (10 mL) was slowly introduced at 50 °C for 2 h, followed by adding GO (0.5 g). The resulting suspension was heated and kept at 55 °C for 5 h. After that, the mixture was filtered and washed with acetone to remove free APTES and hexamethyldisiloxane. Finally, the resulting crude solid was dried at 60 °C for 12 h to produce hyperbranched polysiloxane grafted GO, coded as HBP@GO.

2.3. Synthesis of new hybrid based on HBP@GO and MnF

Imidazole (1.28 g), HBP@GO (0.36 g), 4,4′-dicarboxydiphenyl ether (5.2 g), KOH (2.2 g) and deionized water (140 mL) were thoroughly blended under ultrasound for 30 min to obtain a mixture, into which a solution consisting of deionized water (20 mL) and $Mn(OAC)_2{\cdot}4H_2O$ (4.92 g) was added, followed by maintaining at 75 °C for 24 h with stirring. After cooling to room temperature, obtained solid was washed with water and then dried at 75 °C. The obtained product was the target hybrid, coded as HBP@GO/MnF, in which the content of HBP@GO was 5 wt%.

MnF as reference was also prepared according to above procedure without the addition of HBP@GO.

2.4. Preparation of cured resins

HBP@GO/MnF and BCy resin with different weight ratios (Table 1) were thoroughly blended at 80 °C for 10 min, followed by heating and keeping at 130 °C for 15 min to get a prepolymer. After degassed at 120 °C for 30 min, the prepolymer was cured and post-cured following the cycles of 130 °C/2 h, 150 °C/2 h, 180 °C/2 h, 200 °C/2 h and 220 °C/4 h, successively. After naturally cooling down to room temperature, a cured resin was obtained, its specific code is given in Table 1.

Using above procedure, cured BCy resin without adding fillers was fabricated.

For better comparison, fully cured BCy resin coded as f-BCy was fabricated using the conventional full curing procedure [31], it was 150 °C/2 h + 180 °C/2 h + 200 °C/2 h + 220 °C/2 h + 240 °C/4 h.

2.5. Characterization

The content of $-NH_2$ group (Q_{NH2}) of HBP@GO/MnF was determined using titrimetric method. 0.1 g of HBP@GO/MnF was mixed with excessive HCl solution (0.089 mol/L) to obtain a suspension, of which the pH value was adjusted to 5.0 through adding 0.1 M sodium hydroxide solution. The Q_{NH2} value (4.8×10^{-4} mol/g) of HBP@GO/MnF was then calculated using Eqn (1).

$$Q_{NH_2} = \frac{C_1 V_1 - C_2 V_2}{m} \quad (1)$$

where $C_1 = 0.089$ mol/L, V_1 is volume of HCl solution; C_2 and V_2 are concentration and volume of sodium hydroxide solution; m is quantity of HBP@GO/MnF.

Axis Ultra DID-type X-ray photoelectron Spectrometer (XPS) with a Monochromatic Al-Kα radiation ($h\nu = 1486.6$ eV) from Shimadzu in Japan was employed to characterize structures of fillers.

A fourier transform infrared (FTIR) spectrophotometer (Nicolet-5700, USA) was utilized to characterize chemistry of fillers. The wavenumber resolution was 2 cm^{-1} and spectra were recorded from 4000 to 600 cm^{-1}.

X-ray diffraction (XRD) patterns from 5 to 80° of various fillers were recorded on a Rigaku D/Max diffractometer with Cu-Kα radiation ($\lambda = 1.54$ Å) made in Rigaku Co., Ltd., Japan. The scanning rate was 2°·min^{-1}.

Surfaces of fillers were observed using a transmission electron microscopy (TEM, Hitachi H800) from Japan with an acceleration voltage of 100 kV.

Thermogravimetric (TG) analyses were conducted on a TA Instrument (Discovery TGA, USA) under a nitrogen atmosphere with a flowing rate of 10 mL·min^{-1}. The test temperature varied from 25 to 800 °C with a heating rate of 10 °C·min^{-1}.

A differential scanning calorimetry (DSC, Q200, TA, USA) was used to study the curing property of each prepolymer from 50 to 400 °C under a nitrogen atmosphere with a flowing rate of 50 mL·min^{-1} and a heating rate of 10 °C·min^{-1}.

A Leica DMLM optical microscope was employed to investigate the dispersion of HBP@GO/MnF in BCy resin.

A Q800 dynamic mechanical analyzer (DMA) from TA Instrument in USA was employed to analyze dynamic mechanical properties with a single cantilever bending mode from 30 to 350 °C. The heating rate was 3 °C·min^{-1}, the frequency was 1 Hz, and the dimensions of each sample were $(35 \pm 0.02) \times (13 \pm 0.02) \times (3 \pm 0.02)$ mm^3.

According to ASTM D5045, fracture toughness (K_{IC}) was measured in a single-edge-notch-bending (SENB) method using an electronic universal testing machine (WDW, Shenzhen, China). The crosshead speed was 0.5 mm·min^{-1}. According to Chinese Standard GB/T2571-95, impact strengths of resins were measured with a JGL-5 universal tester made in Shenzhen, China. With the procedure of GB/T2570-95, flexural properties were tested using an electronic universal testing machine (WDW, Shenzhen, China). Flexural strength and modulus of each sample were calculated using Eqn (2) and Eqn (3), respectively. The crosshead speed was 2 mm·min^{-1}. For each property of a system, the average value based on at least five effective data was calculated as the final value.

$$\sigma_f = \frac{3P \cdot L}{2b \cdot h^2} \quad (2)$$

$$E_f = \frac{L^3 \cdot \Delta P}{4b^3 \cdot \Delta f} \quad (3)$$

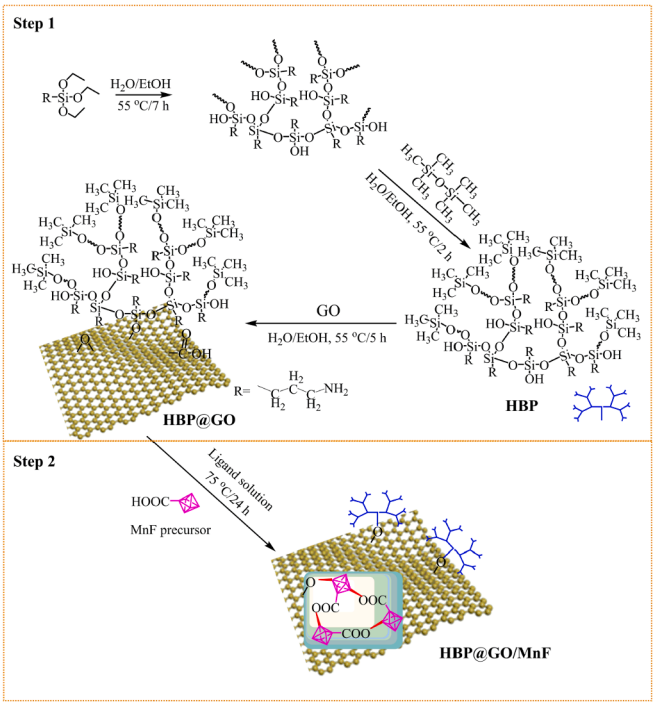

Fig. 1. Synthesizing HBP@GO/MnF hybrid.

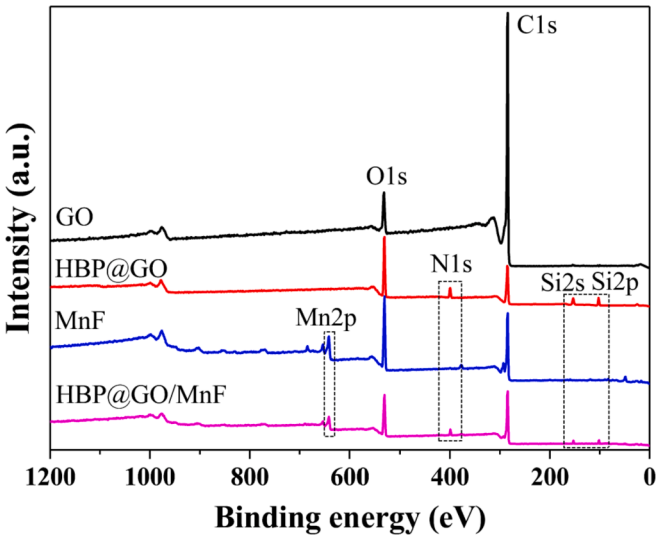

Fig. 2. XPS spectra of GO, HBP@GO, MnF and HBP@GO/MnF.

where P is break force (N); L is support span (mm); b is width of each specimen (mm); h is thickness of each specimen (mm); ΔP is difference in flexural stress between two selected strain points (N); Δf is difference between two selected strain points (mm).

Dielectric properties of each sample with dimensions of $(2.5 \pm 0.1) \times (25 \pm 1) \times (25 \pm 1)$ mm^3 were tested at room temperature over the frequency from 1 to 10^4 Hz on a broadband dielectric spectrometer (Novocontrol Concept 80, Germany).

3. Results and discussion

3.1. Synthesis and structure of HBP@GO/MnF hybrid

A two-step procedure was designed to synthesize HBP@GO/MnF hybrid (Fig. 1), which included grafting HBP on surfaces of GO sheets,

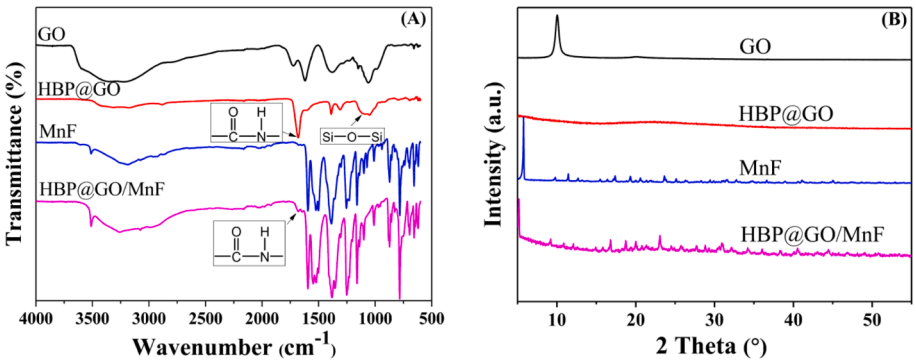

Fig. 3. FTIR spectra (A) and XRD patterns (B) of GO, HBP@GO, MnF and HBP@GO/MnF.

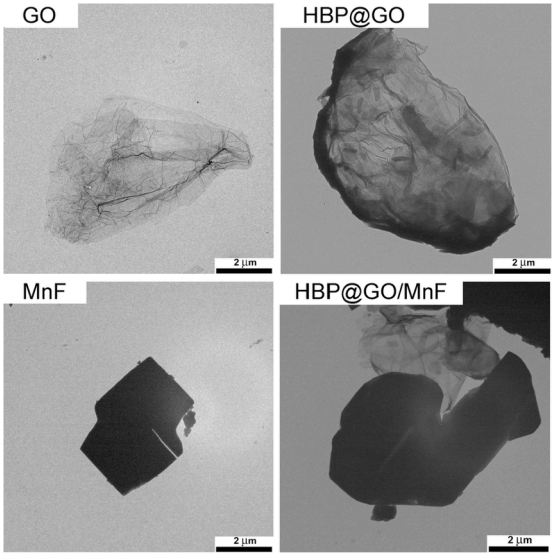

Fig. 4. TEM images of GO, HBP@GO, MnF and HBP@GO/MnF.

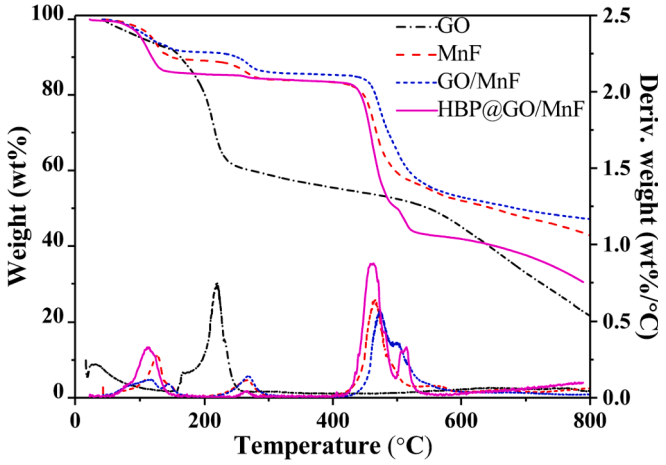

Fig. 5. TG analyses of GO, MnF, GO/MnF and HBP@GO/MnF.

followed by coordinating with Mn^{2+} in the MnF precursors.

Fig. 2 provides survey XPS spectra of GO, HBP@GO, MnF and HBP@GO/MnF. Two obvious peaks belonging to O 1s (532 eV) and C 1s (284 eV) appear in the XPS spectrum of GO, which are also observed in the spectrum of HBP@GO, besides, there are new peaks representing N 1s (400 eV), Si 2s (153 eV) and Si 2p (102 eV), suggesting that HBP has been successfully grafted on GO. XPS survey of HBP@GO/MnF shows a new peak of Mn 2p (641 eV) compared to that of HBP@GO due to hybridization of MnF. These results verify the successful functionalization of GO sheets with HBP as well as the combination of HBP@GO and MnF.

More evidence of the successful preparation of HBP@GO/MnF can be demonstrated by FTIR spectra and XRD patterns. Characteristic peaks of epoxy group (1060 cm^{-1}), C=O (1738 cm^{-1}) and –OH (3420 cm^{-1}) [32] are found in both FTIR spectra of GO and HBP@GO (Fig. 3A), while vibration peaks assigning to amide (1660 cm^{-1}) and Si–O–Si (1055 cm^{-1}) appear in FTIR spectrum of HBP@GO, proving the occurrence of hydrolyzation among alkoxy groups in APTES as well as amidation reaction between amine of APTES and carboxyl of GO.

A sharp peak at $2\theta = 10°$ is found in the XRD pattern of GO (Fig. 3B), which does not appear in the pattern of HBP@GO, suggesting that grafting HBP on GO disorders the stacking structure of GO sheets and exfoliates GO sheets, this also demonstrates that GO has been effectively functionalized by HBP.

During the preparation of HBP@GO/MnF (Fig. 1, Step 2), Mn^{2+} is coordinated with oxygen-containing groups on HBP@GO sheets. HBP@GO/MnF has similar FTIR spectrum as MnF (Fig. 3A), this result and the appearance of characteristic peak of amide (1660 cm^{-1}) confirm that HBP@GO and MnF are chemically bonded together to produce HBP@GO/MnF hybrid. In the case of XRD pattern, MnF exhibits the same one as that found for the single crystal for $Mn_2(OH)(H_2O)_6\{C_{12}H_8O(COO)_2\}_2$ [33]. HBP@GO/MnF has similar pattern as MnF (Fig. 3B), which not only suggests the formation of linkages between Mn^{2+} and ligands, but also demonstrates that the structure of MnF remains intact in the presence of HBP@GO. It is noteworthy that the sharp peak at $2\theta = 5.77°$ corresponding to the width (15.3 Å) of MnF shifts toward 5.19° (d = 17.0 Å) when MnF has been coordinated with HBP@GO, indicating that there are strong interactions between oxygen-containing groups on HBP@GO and Mn^{2+}.

TEM images show that GO consists of very thin nanosheets with some wrinkles and folded regions (Fig. 4). Compared with GO, HBP@GO exhibits less transparent nanosheets, where some black regions are observed. This is because HBP has been grafted onto GO from both sides. In contrast, MnF exhibits a rather different morphology that is non-transparent square with distinct edges and corners. In the case of HBP@GO/MnF hybrid, HBP@GO sheets are linked with MnF, resulting in less sharp edges and corners of MnF.

In order to evaluate the coordination effect of various hybrids, TG analyses of GO, MnF, GO/MnF and HBP@GO/MnF were performed. As shown in Fig. 5, thermal decomposition of GO starts before 100 °C due to the loss of absorbed moisture [34]. GO shows a sharp degradation from 150 to 270 °C, resulting from the decomposition of compounds containing oxygen groups (hydroxy, carboxy and epoxy) between GO layers. A slow and gradual weight loss occurs when the temperature increases to 300 °C because of the decomposition of more thermally stable cyclic compounds on GO, such as anhydrides, lactones or lactols [35].

Different from GO, MnF and GO/MnF show three distinct thermal

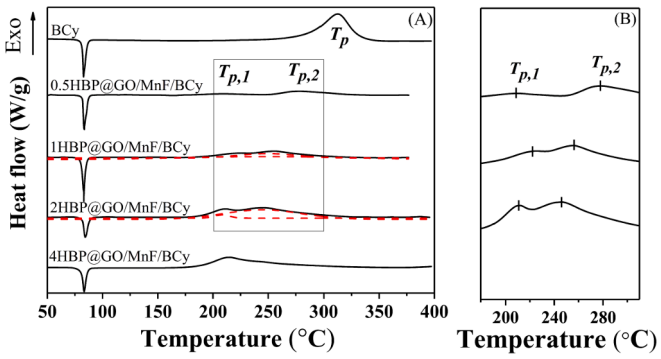

Fig. 6. DSC curves of BCy and HBP@GO/MnF/BCy prepolymers (A) and enlarged curves from 180 to 310 °C for HBP@GO/MnF/BCy prepolymers (B).

Table 2
Curing data of BCy and HBP@GO/MnF/BCy prepolymers.[a]

Prepolymer	T_m (°C)	T_i (°C)	T_p		T_f (°C)
			$T_{p,1}$ (°C)	$T_{p,2}$ (°C)	
BCy	83	268	313		343
0.5HBP@GO/MnF/BCy	83	204	208	278	320
1HBP@GO/MnF/BCy	83	197	212	249	303
2HBP@GO/MnF/BCy	85	182	208	246	313
4HBP@GO/MnF/BCy	84	177	216		296

[a] T_i, $T_{p,1}$, $T_{p,2}$ and T_f refer to the initial temperature of exothermic peak, the first peak temperature, the second peak temperature and end temperature of exothermic peak, respectively.

decomposition steps divided by three DTG peaks, they are the removal of coordination water at 100 °C, the decomposition of compounds containing oxygen groups at 220 °C and the decomposition of organic linker of MnF at 460 °C, respectively. HBP@GO/MnF hybrid also displays three thermal decomposition steps, however, it is worth noting that the decomposition of HBP@GO/MnF at 220 °C is much smaller than those of MnF and GO/MnF hybrid, indicating that oxygen-containing groups between HBP@GO layers have been completely coordinated with Mn^{2+} in the MnF precursors.

3.2. Curing property

Fig. 6 gives DSC curves of BCy and HBP@GO/MnF/BCy prepolymers, the corresponding data are summarized in Table 2. Each prepolymer has a similar melting temperature at *ca.* 83 °C. BCy prepolymer has a symmetric exothermic peak centered at 313 °C, referring to the reaction of producing triazine rings. With the addition of 0.5 wt% HBP@GO/MnF, DSC curve exhibits two peaks centered at 208 °C and 278 °C (Fig. 6B), proving that HBP@GO/MnF has a catalytic effect on BCy. As the loading of HBP@GO/MnF increases, the peak at high temperature moves toward low temperature, and two exothermic peaks gradually overlap. Eventually, DSC curve of 4HBP@GO/MnF/BCy resin only shows one exothermic peak, of which the peak temperature is 216 °C, about 97 °C lower than that of BCy prepolymer. The unique structure of HBP@GO/MnF is responsible for these results. Specifically, HBP@GO/MnF integrates Mn^{2+} and abundant active hydrogen (amino, hydroxy and carboxy) into one hybrid, so metal-π intermediate is easily formed between Mn^{2+} and BCy, and thus playing an efficient catalytic effect on curing BCy as described in Fig. 7, leading to a lower curing temperature. In addition, the grafted HBP endows HBP@GO/MnF with

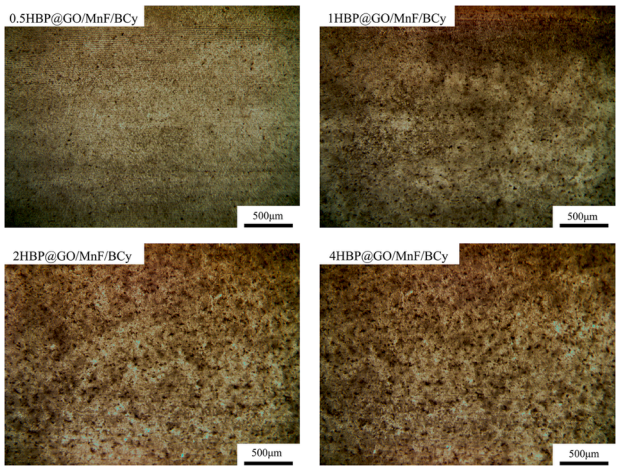

Fig. 8. Optical microscope images of HBP@GO/MnF/BCy resins (thickness = 2 μm).

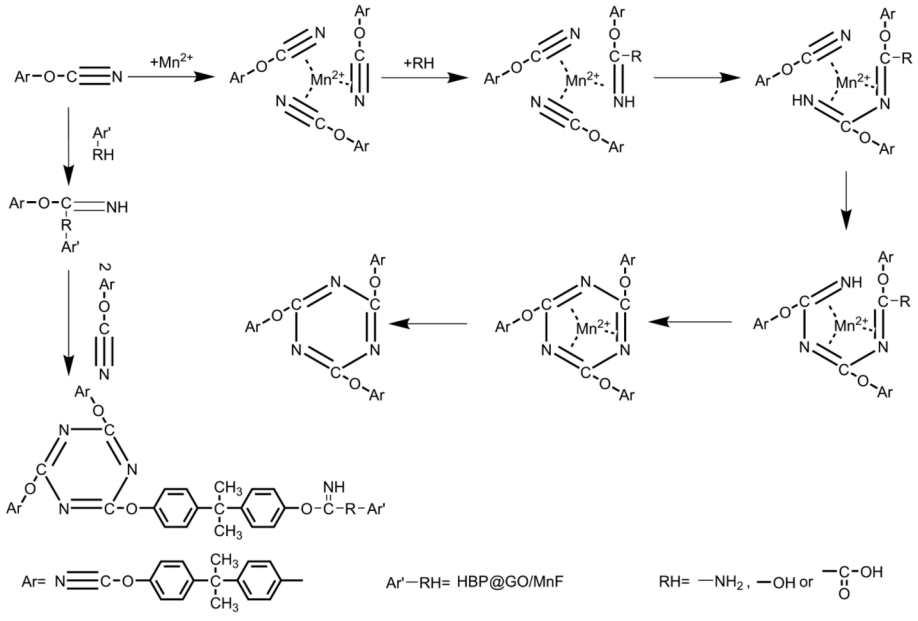

Fig. 7. The curing mechanism of HBP@GO/MnF/BCy.

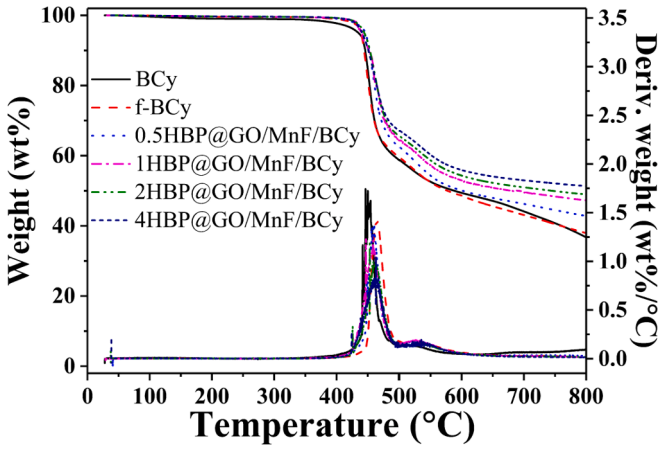

Fig. 9. TG and DTG curves of cured resins.

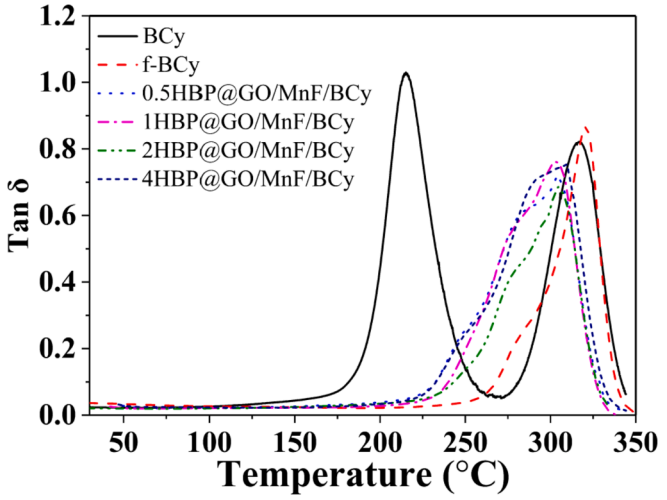

Fig. 10. Temperature-dependent loss factors of cured resins.

better compatibility than GO and MnF, and thus guaranteeing good dispersion of HBP@GO/MnF in BCy resin (Fig. 8) as well as good interfacial interactions between HBP@GO/MnF and BCy resin.

3.3. Thermal properties

Thermal properties of a thermosetting resin usually include thermogravimetric property [36] and glass transition temperature (T_g) [37]. Previous researches showed that the formation of copolymer with BCy and presence of fillers reduced initial degradation temperature (T_{di}) [16,38]. However, this phenomenon is not found in HBP@GO/MnF/BCy resins (Fig. 9), instead, all HBP@GO/MnF/BCy resins exhibit higher T_{di} values than both BCy and f-BCy resins, although f-BCy resin shows improved heat resistance after complete curing. There are three reasons to explain these attractive results. The first is the good chemical interfacial interaction between HBP@GO/MnF and BCy resin, which makes the latter two factors play bigger roles. The second is that the effective role of HBP@GO/MnF on catalyzing the curing of BCy promotes the formation of triazine ring structure, and thus improving the thermal resistance. The third is that HBP@GO/MnF has lamellar structure, which acts as heat barrier to protect the decomposition of resins.

Fig. 9 also shows the char yield (Y_c) of all cured resins. Both BCy and f-BCy resins have similar Y_c. However, Y_c of each HBP@GO/MnF/BCy resin is not only larger than those of both BCy and f-BCy resins, but also bigger than corresponding calculated value using the addition rule, demonstrating that HBP@GO/MnF plays a catalytic role on forming char, and thus producing a char layer to prevent resins from the attack of transmitted heat.

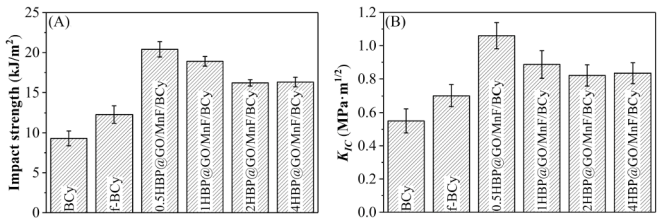

Fig. 11. Impact strengths (A) and K_{IC} (B) of cured resins.

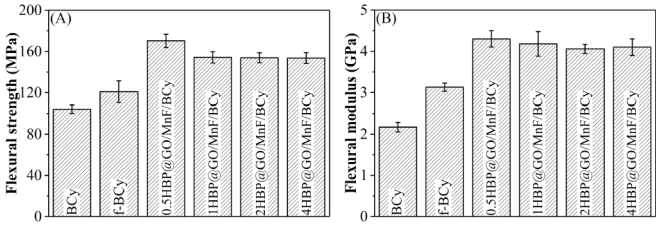

Fig. 12. Flexural strengths (A) and moduli (B) of cured resins.

Fig. 10 shows temperature dependence of loss factor (tan δ) of each cured resin. f-BCy resin shows a single peak at 321 °C, indicating that f-BCy resin is completely cured and structure is uniform. In the curve of BCy resin, two separate peaks appear at 215 °C and 317 °C, so crosslinked BCy resin has non-uniform structure, which includes areas with low T_g and that with high T_g; in other words, BCy resin has not been completely crosslinked after postcuring at 220 °C for 4 h. Differently, each HBP@GO/MnF/BCy resin shows one wide peak at high temperature, proving that HBP@GO/MnF has great ability of promoting complete and uniform curing.

3.4. Mechanical properties

Toughening is the most important issue for thermosetting resins including BCy resin. For our project reported herein, investigating toughness has additional meaning because catalyzing curing of thermosetting resins usually tends to degrade toughness [39], in other words, it is difficult to simultaneously achieve toughening and reducing curing temperature of thermosetting resins.

The impact strengths and plane strain fracture toughnesses of cured resins are depicted in Fig. 11. Compared with BCy and f-BCy resins, all HBP@GO/MnF/BCy resins exhibit greatly increased impact strengths, in particular, the impact strength of 0.5HBP@GO/MnF/BCy resin is 2.2 and 1.7 times of those of BCy resin and f-BCy resin (Fig. 11A), respectively. Similar results are also found in fracture toughness (Fig. 11B), proving that HBP@GO/MnF has efficient toughening effect on BCy resin.

Flexural strength is a unique index for integrated mechanical properties of materials because of multiple kinds of loadings [40]. Fig. 12A shows that the flexural strength of 0.5HBP@GO/MnF/BCy resin reaches 170 MPa, about 1.6 and 1.4 times of those for BCy resin and f-BCy resin, respectively. This result is derived from both toughening and strengthening effects of HBP@GO/MnF.

In many circumstances, flexible chain segments have been introduced to toughen thermosetting resins, however, good mobility makes flexible chain segments easier to deform under external force, and leading to decreased stiffness. In other words, achieving toughening without declining stiffness is important for developing high performance resins. The stiffness of thermosetting resins can be reflected by flexural modulus [41]. As shown in Fig. 12B, with 0.5 wt% HBP@GO/MnF into BCy resin, the flexural modulus is increased by 98% for BCy resin and

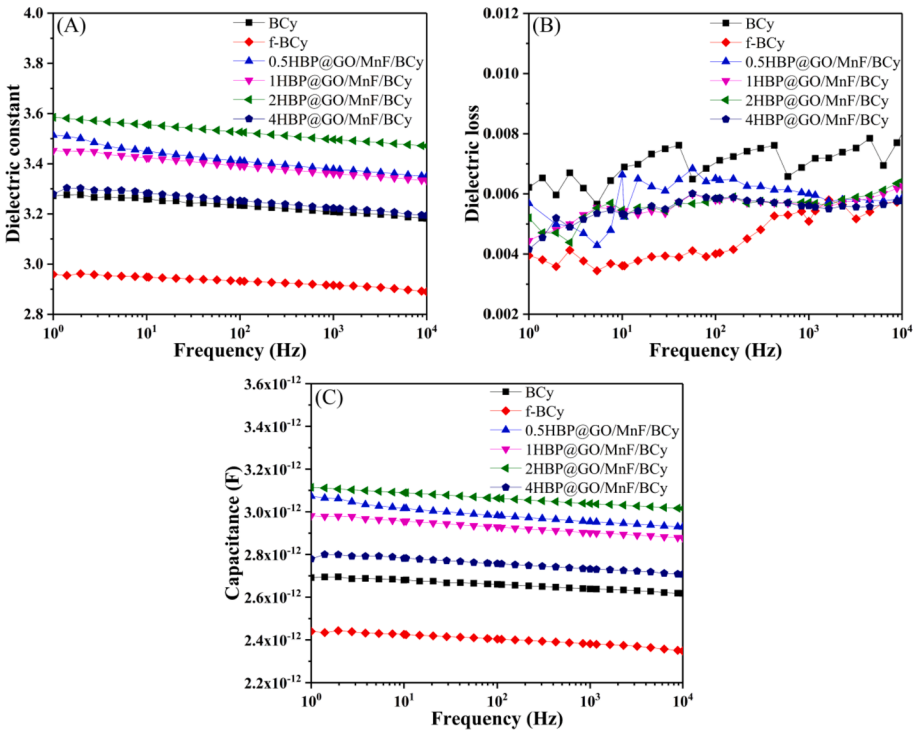

Fig. 13. Overlay plots of dielectric constants (A), dielectric losses (B) and capacitances (C) at different frequencies of cured resins.

37% for f-BCy resin, and the former is much higher than the enhancement (10–77%) reported in literature with the same loading of rigid inorganic nano-fillers [6,7,42], so HBP@GO/MnF has more significant strengthening effect than other nano-fillers. The greatly improved stiffness of HBP@GO/MnF/BCy resins is attributed to the high modulus of HBP@GO/MnF and the increased content of triazine rings in the crosslinked network.

3.5. Dielectric properties

Compared with other thermosetting resins, low dielectric loss (0.002–0.008) is the biggest advantage owned by BCy resin [43], so it is necessary for modified BCy resins to remain this merit.

Fig. 13 provides dielectric property-frequency plots of BCy, f-BCy and HBP@GO/MnF/BCy resins. It is expected to found that f-BCy shows the lowest dielectric constant and loss, because fully cured f-BCy resin has more symmetrical triazine-ring structure. Interestingly, HBP@GO/MnF/BCy resins exhibit little higher dielectric constant but lower dielectric loss than BCy resin, this is because HBP@GO/MnF/BCy resins have more triazine-ring structure owing to the catalysis of HBP@GO/MnF. The different change trend in dielectric constant and loss suggests that there are other factors making contribution to dielectric constant because factors affecting dielectric constant are generally thought to play the same role on dielectric loss [44].

The frequency-dependent capacitances of BCy and HBP@GO/MnF/BCy resins were recorded and shown in Fig. 13C. At the same frequency, HBP@GO/MnF/BCy resins have higher capacitance than BCy resin. This result is expected as HBP@GO/MnF has good dispersion in BCy resin, leading to more capacitors and thus higher dielectric constant.

4. Conclusions

Through grafting HBP and hybridizing MnF on surface of GO, a new hybrid (HBP@GO/MnF) has been developed, which can not only simultaneously reduce curing temperature and greatly toughen BCy resin, but also strengthen the biggest advantage of BCy resin, that is, reducing dielectric loss. With only 0.5 wt% of HBP@GO/MnF, HBP@GO/MnF/BCy system shows about 120%, 93%, 60% and 98% higher impact strength, fracture toughness, flexural strength and modulus than pure BCy resin, respectively. In addition, HBP@GO/MnF/BCy resins have better mechanical properties and higher heat resistance than fully cured BCy resin. These outstanding integrated performances of HBP@GO/MnF/BCy resins are originated from the unique structure of HBP@GO/MnF. HBP grafted on GO integrates Mn^{2+} and abundant active hydrogen into one hybrid, and thus resulting in a high-efficiency intrinsic-type catalyst for curing BCy; in addition, HBP endows HBP@GO/MnF with good interfacial interactions with BCy resin and good dispersion in BCy resin, therefore, the toughening and catalyzing effects of fillers are fully exerted.

Acknowledgment

This work was financially supported by Key Major Program of Natural Science Fundamental Research Project of Jiangsu Colleges and Universities (Grant No. 18KJA430013), National Natural Science Foundation of China (Grant No. 51873135) and Priority Academic Program Development of Jiangsu Higher Education Institutions (PAPD).

References

[1] L.A. Rodriguez, C. García, L.R. Grace, Long-term durability of a water-contaminated quartz-reinforced bismaleimide laminate, Polym. Compos. 39 (2018) 2643–2649. https://doi.org/10.1002/pc.24255.

[2] T.D. Mekuria, Z. Chunhong, L. Yingnan, D. El Din Fouad, K. Lv, M. Yang, Y. Zhou, Surface modification of nano-silica by diisocyanates and their application in polyimide matrix for enhanced mechanical, thermal and water proof properties, Mater. Chem. Phys. 225 (2019) 358–364. https://doi.org/10.1016/j.matchemphys.2018.12.107.

[3] X. Fan, J.-T. Miao, L. Yuan, Q. Guan, A. Gu, G. Liang, Preparation and origin of thermally resistant biobased epoxy resin with low internal stress and good UV resistance based on SiO2 hybridized cellulose for light emitting diode encapsulation, Appl. Surf. Sci. 447 (2018) 315–324. https://doi.org/10.1016/j.apsusc.2018.03.229.

[4] S. Zhang, X. Li, H. Fan, Q. Fu, Y. Gu, Epoxy nanocomposites: improved thermal and dielectric properties by benzoxazinyl modified polyhedral oligomeric silsesquioxane, Mater. Chem. Phys. 223 (2019) 260–267. https://doi.org/10.1016/j.matchemphys.2018.10.048.

[5] T. Na, S. Che, Y. Sun, X. Liu, J. Hao, C. Zhao, Synthesis of a novel biphenyl epoxy resin and its hybrid composite with high thermal conductivity, J. Appl. Polym. Sci. 136 (2019) 47078. https://doi.org/10.1002/app.47078.
[6] X. Gu, Z. Zhang, L. Yuan, G. Liang, A. Gu, Developing high performance cyanate ester resin with significantly reduced postcuring temperature while improved toughness, rigidity, thermal and dielectric properties based on manganese-Schiff base hybridized graphene oxide, Chem. Eng. J. 298 (2016) 214–224. https://doi.org/10.1016/j.cej.2016.04.031.
[7] H. Wang, L. Yuan, G. Liang, A. Gu, Tough and thermally resistant cyanate ester resin with significantly reduced curing temperature and low dielectric loss based on developing an efficient graphene oxide/Mn ion metal–organic framework hybrid, RSC Adv. 6 (2016) 3290–3300. https://doi.org/10.1039/C5RA21765B.
[8] A. Vashchuk, A. Rios de Anda, O. Starostenko, O. Grigoryeva, P. Sotta, S. Rogalsky, P. Smertenko, A. Fainleib, D. Grande, Structure−Property relationships in nanocomposites based on cyanate ester resins and 1-heptyl pyridinium tetrafluoroborate ionic liquid, Polymer 148 (2018) 14–26. https://doi.org/10.1016/j.polymer.2018.06.015.
[9] A. Zegaoui, M. Derradji, R.-k. Ma, W.-a. Cai, A. Medjahed, W.-b. Liu, A.Q. Dayo, J. Wang, G.-x. Wang, Influence of fiber volume fractions on the performances of alkali modified hemp fibers reinforced cyanate ester/benzoxazine blend composites, Mater. Chem. Phys. 213 (2018) 146–156. https://doi.org/10.1016/j.matchemphys.2018.04.012.
[10] L. Tang, J. Dang, M. He, J. Li, J. Kong, Y. Tang, J. Gu, Preparation and properties of cyanate-based wave-transparent laminated composites reinforced by dopamine/POSS functionalized Kevlar cloth, Compos. Sci. Technol. 169 (2019) 120–126. https://doi.org/10.1016/j.compscitech.2018.11.018.
[11] Y. Li, G. Xu, Y. Guo, T. Ma, X. Zhong, Q. Zhang, J. Gu, Fabrication, proposed model and simulation predictions on thermally conductive hybrid cyanate ester composites with boron nitride fillers, Compos. Appl. Sci. Manuf. 107 (2018) 570–578. https://doi.org/10.1016/j.compositesa.2018.02.006.
[12] X. Chen, J. Wang, S. Huo, S. Yang, B. Zhang, H. Cai, Study on properties of flame-retardant cyanate esters modified with DOPO and triazine compounds, Polym. Adv. Technol. 29 (2018) 2574–2582. https://doi.org/10.1002/pat.4368.
[13] K. Wang, G. Zhu, Y. Wang, F. Ren, Thermal and shape memory properties of cyanate/polybutadiene epoxy/polysebacic polyanhydride copolymer, J. Appl. Polym. Sci. 132 (2015) 42045. https://doi.org/10.1002/app.42045.
[14] M.D. Martin, M. Ormaetxea, I. Harismendy, P.M. Remiro, I. Mondragon, Cure chemo-rheology of mixtures based on epoxy resins and ester cyanates, Eur. Polym. J. 35 (1999) 57–68. https://doi.org/10.1016/S0014-3057(98)00095-0.
[15] S. Zhang, Y. Yan, X. Li, H. Fan, Q. Ran, Q. Fu, Y. Gu, A novel ultra low-k nanocomposites of benzoxazinyl modified polyhedral oligomeric silsesquioxane and cyanate ester, Eur. Polym. J. 103 (2018) 124–132. https://doi.org/10.1016/j.eurpolymj.2018.03.013.
[16] J. Ma, X. Lei, Y. Wang, Y. Sun, Toughening modification of cyanate ester with amino-terminated polyoxypropylene, Iran, Polym. J. 27 (2018) 145–151. https://doi.org/10.1007/s13726-017-0594-1.
[17] H.C.Y. Koh, J. Dai, E. Tan, W. Liang, Catalytic effect of 2,2′-diallyl bisphenol A on thermal curing of cyanate esters, J. Appl. Polym. Sci. 101 (2006) 1775–1786. https://doi.org/10.1002/app.23533.
[18] Z. Zhang, G. Liang, X. Wang, S. Adhikari, J. Pei, Curing behavior and dielectric properties of amino-functionalized polyhedral oligomeric silsesquioxane/cyanate ester resin hybrids, High Perform. Polym. 25 (2013) 427–435. https://doi.org/10.1177/0954008312469234.
[19] T. Liu, J. Li, J. Xiao, W. Tian, Thermal and mechanical evaluation of cyanate ester resin catalyzed by nonylphenol and stannous octoate, J. Appl. Polym. Sci. 133 (2016) 43959. https://doi.org/10.1002/app.43959.
[20] L. Yuan, F. Chen, A. Gu, G. Liang, C. Lin, S. Huang, S. Nutt, G. Chen, Y. Gao, Synthesis of poly(urea–formaldehyde) encapsulated dibutyltin dilaurate through the self-catalysis of core materials, Polym. Bull. 71 (2014) 261–273. https://doi.org/10.1007/s00289-013-1059-0.
[21] S. Chandrasekaran, E.B. Duoss, M.A. Worsley, J.P. Lewicki, 3D printing of high performance cyanate ester thermoset polymers, J. Mater. Chem. 6 (2018) 853–858. https://doi.org/10.1039/C7TA09466C.
[22] C.P.R. Nair, C. Gopalakrishnan, K.N. Ninan, Kinetics of zinc octoate/nonylphenol catalysed thermal cure of bisphenol a dicyanate, Polym. Polym. Compos. 9 (2001) 531–539. https://doi.org/10.1177/096739110100900806.
[23] D. Mathew, C.P.R. Nair, K. Krishnan, K.N. Ninan, Catalysis of the cure reaction of bisphenol A dicyanate. A DSC study, J. Polym. Sci., Part A: Polym. Chem. 37 (1999) 1103–1114. https://doi.org/10.1002/(SICI)1099-0518(19990415)37, 8<1103::AID-POLA7>3.0.CO;2-X.
[24] Z. Yang, Y. Shi, Y. Zhang, Q. Cheng, X. Li, C. Zhao, D. Zhang, Different pathways for 4-n-nonylphenol biodegradation by two Aspergillus strains derived from estuary sediment: evidence from metabolites determination and key-gene identification, J. Hazard Mater. 359 (2018) 203–212. https://doi.org/10.1016/j.jhazmat.2018.07.058.
[25] P. Baruah, N. Karak, Bio-based tough hyperbranched epoxy/graphene oxide nanocomposite with enhanced biodegradability attribute, Polym. Degrad. Stabil. 129 (2016) 26–33. https://doi.org/10.1016/j.polymdegradstab.2016.03.021.
[26] G.G. Kaya, E. Yilmaz, H. Deveci, Sustainable bean pod/calcined kaolin reinforced epoxy hybrid composites with enhanced mechanical, water sorption and corrosion resistance properties, Constr. Build. Mater. 162 (2018) 272–279. https://doi.org/10.1016/j.conbuildmat.2017.12.046.
[27] Y. Wang, S. Zhou, H. Du, Investigation of dielectric properties of polymer composites with kaolin, J. Mater. Sci. Mater. Electron. 29 (2018) 12360–12365. https://doi.org/10.1007/s10854-018-9349-9.
[28] K.-Y. Li, C.-F. Kuan, H.-C. Kuan, C.-H. Chen, M.-Y. Shen, J.-M. Yang, C.-L. Chiang, Preparation and properties of novel epoxy/graphene oxide nanosheets (GON) composites functionalized with flame retardant containing phosphorus and silicon, Mater. Chem. Phys. 146 (2014) 354–362. https://doi.org/10.1016/j.matchemphys.2014.03.037.
[29] C. Tang, H. Yan, S. Li, L. Bai, Q. Lv, Effects of novel polyhedral oligomeric silsesquioxane containing hydroxyl group and epoxy group on the dicyclopentadiene bisphenol dicyanate ester composites, Polym. Test. 59 (2017) 316–327. https://doi.org/10.1016/j.polymertesting.2017.02.014.
[30] W.S. Hummers, R.E. Offeman, Preparation of graphitic oxide, J. Am. Chem. Soc. 80 (1958) 1339, 1339, https://doi.org/10.1021/ja01539a017.
[31] L. Zhao, L. Yuan, G. Liang, A. Gu, Novel tough and thermally stable cyanate ester resins with high flame retardancy, low dielectric loss and constant based on a phenolphthalein type polyarylether sulfone, RSC Adv. 5 (2015) 58989–59002. https://doi.org/10.1039/C5RA10670B.
[32] S.K. Ujjain, V. Sahu, R.K. Sharma, G. Singh, High performance, all solid state, flexible supercapacitor based on ionic liquid functionalized graphene, Electrochim. Acta 157 (2015) 245–251. https://doi.org/10.1016/j.electacta.2015.01.061.
[33] P. Mahata, A. Sundaresan, S. Natarajan, The role of temperature on the structure and dimensionality of MOFs: an illustrative study of the formation of manganese oxy-bis(benzoate) structures, Chem. Commun. 0 (2007) 4471–4473. https://doi.org/10.1039/B708060C.
[34] A. Molla, Y. Li, B. Mandal, S.G. Kang, S.H. Hur, J.S. Chung, Selective adsorption of organic dyes on graphene oxide: theoretical and experimental analysis, Appl. Surf. Sci. 464 (2019) 170–177. https://doi.org/10.1016/j.apsusc.2018.09.056.
[35] F. Najafi, M. Rajabi, Thermal gravity analysis for the study of stability of graphene oxide–glycine nanocomposites, Int. Nano Lett. 5 (2015) 187–190. https://doi.org/10.1007/s40089-015-0154-7.
[36] M. Abouhamzeh, J. Sinke, Effects of fusion bonding on the thermoset composite, Compos. Part A:Appl. Sci. Manuf. 118 (2019) 142–149. https://doi.org/10.1016/j.compositesa.2018.12.031.
[37] J. Zhou, J.P. Lucas, Hygrothermal effects of epoxy resin. Part II: variations of glass transition temperature, Polymer 40 (1999) 5513–5522. https://doi.org/10.1016/S0032-3861(98)00791-5.
[38] Y. Cheng, B. Xia, C. Fang, L. Yang, Structure, mechanical and thermal properties of BMI/E-44/CNTs ternary composites via amination method, J. Mater. Sci. Technol. 33 (2017) 1187–1194. https://doi.org/10.1016/j.jmst.2017.04.013.
[39] J. Zhang, S. Chen, Q. He, P. Guo, Z. Xu, D. Zhang, Toughening benzoxazines with hyperbranched polymeric ionic liquids: effect of cations and anions, React. Funct. Polym. 133 (2018) 37–44. https://doi.org/10.1016/j.reactfunctpolym.2018.10.002.
[40] C. Dong, I.J. Davies, Flexural and tensile strengths of unidirectional hybrid epoxy composites reinforced by S-2 glass and T700S carbon fibres, Mater. Des. 54 (1980–2015) (2014) 955–966. https://doi.org/10.1016/j.matdes.2013.08.087.
[41] J. Hoffman, J. Middleton, M. Kumosa, Effect of a surface coating on flexural performance of thermally aged hybrid glass/carbon epoxy composite rods, Compos. Sci. Technol. 106 (2015) 141–148. https://doi.org/10.1016/j.compscitech.2014.11.010.
[42] Z. Zhang, L. Yuan, Q. Guan, G. Liang, A. Gu, Synergistically building flame retarding thermosetting composites with high toughness and thermal stability through unique phosphorus and silicone hybridized graphene oxide, Compos. Appl. Sci. Manuf. 98 (2017) 174–183. https://doi.org/10.1016/j.compositesa.2017.03.025.
[43] J. Gu, Y. Li, C. Liang, Y. Tang, L. Tang, Y. Zhang, J. Kong, H. Liu, Z. Guo, Synchronously improved dielectric and mechanical properties of wave-transparent laminated composites combined with outstanding thermal stability by incorporating iysozyme/POSS functionalized PBO fibers, J. Mater. Chem. C 6 (2018) 7652–7660. https://doi.org/10.1039/C8TC02391C.
[44] R. Wei, L. Tu, Y. You, C. Zhan, Y. Wang, X. Liu, Fabrication of crosslinked single-component polyarylene ether nitrile composite with enhanced dielectric properties, Polymer 161 (2019) 162–169. https://doi.org/10.1016/j.polymer.2018.12.017.